Distribution of Time Scales Induces Slow Dynamics and Elastic Hysteresis in Sandstones: A Model of Non-equilibrium Strain

Rock Mechanics and Rock Engineering
https://doi.org/10.1007/s00603-025-04668-5

ORIGINAL PAPER

Distribution of Time Scales Induces Slow Dynamics and Elastic Hysteresis in Sandstones: A Model of Non-equilibrium Strain

Radovan Zeman[1,2] · **Jan Kober**[1] · **Marco Scalerandi**[3]

Received: 29 October 2024 / Accepted: 20 May 2025

Abstract

Elasticity in consolidated granular materials exhibits non-classical nonlinearity and slow dynamics. These effects are typically analyzed through separate experimental methods and theoretical models. Our research aims to unify these descriptions by introducing a model based on non-equilibrium strain, incorporating a wide range of relaxation times to account for both fast nonlinear effects and slow conditioning and relaxation of elastic properties. Utilizing observations from dynamic acoustoelastic testing of sandstone, we propose a time-delay model that accurately reflects the observed experimental behaviors, including log-time relaxation and hysteresis. Our findings indicate that the slow and fast dynamics in sandstone are intrinsically coupled, and the model provides a comprehensive framework for understanding these complex interactions. This model, which is validated by fitting experimental data including conditioning loops and relaxation curves, offers a tool for predicting the elastic behavior under various loading conditions.

Highlights

- A model based on non-equilibrium strain including a wide range of relaxation times allows for the simultaneous description of fast nonlinear effects and slow dynamics in sandstones.
- The model shows that the intrinsic coupling of slow and fast dynamics in sandstones leads to the observed experimental behaviors, such as log-time relaxation and hysteresis.
- The model is validated by quantitatively reproducing experimental observations from dynamic acoustoelastic testing (DAET), accurately reflecting conditioning loops and relaxation curves.

Keywords Nonlinear elasticity · Hysteresis · Slow dynamics · Dynamic acoustoelastic testing

1 Introduction

The elastic response of mesoscopic materials is affected by non-classical (hysteretic) nonlinearity and slow dynamics. Usually, these effects were studied separately, leading to the development of independent theoretical descriptions and experimental methods. While non-classical nonlinearity is considered a time-invariant and immediate effect, slow dynamics involves a complex temporal evolution over a wide range of timescales. However, all experimental observations indicate that non-classical nonlinearity and slow dynamics are intrinsically coupled. Thus, the objective here is to define a model to unify the description of slow dynamics and non-classical nonlinearity, linking both to the same physical processes.

✉ Jan Kober
kober@it.cas.cz

Radovan Zeman
rzeman@it.cas.cz

Marco Scalerandi
marco.scalerandi@polito.it

[1] Institute of Thermomechanics, Czech Academy of Sciences, Prague, Czechia

[2] Faculty of Nuclear Sciences and Physical Engineering, Czech Technical University in Prague, Prague, Czechia

[3] DISAT, Condensed Matter Physics and Complex Systems Institute, Politecnico di Torino, Turin, Italy

Published online: 13 August 2025

Several models have been proposed to interpret fast dynamic effects including hysteresis. A common description of non-classical nonlinearity is based on introducing a Preisach–Mayergoyz space distribution of elastic hysterons in analogy with magnetic hysteresis (McCall and Guyer 1994). For a special case of uniform PM space distribution, a widely used hysteretic model was introduced by Van Den Abeele et al. (2001). This hysteretic model involves two coefficients of quadratic and cubic classical nonlinearity and a single coefficient to measure hysteresis. The model captures well most of the observed nonlinear effects: generation of harmonics (Van Den Abeele et al. 2000b), shift of the resonance frequency in nonlinear resonant ultrasound spectroscopy (NRUS) (Van Den Abeele et al. 2000a) and formation of loops in the strain dependence of velocity observed in dynamic acoustoelastic testing (DAET) (Rivière et al. 2013). However, it does not include any time dependence nor any non-equilibrium effect typical of slow dynamics.

At the same time, time-dependent variations of resonant frequency were observed during NRUS testing and called slow dynamics (TenCate and Shankland 1996). Slow dynamics consists of a conditioning phase, when the material modulus decreases during dynamic excitation, and relaxation, when the modulus recovers to the original value. It has been observed that slow dynamic relaxation is a log-time process spanning several time scales (TenCate et al. 2000), which sets it apart from other transient processes like temperature shocks, which follow exponential curves. Such phenomenon was observed for a range of materials and spatial scales, from a single bead contact (Yoritomo and Weaver 2020), unconsolidated (Reichhardt et al. 2015) and consolidated granular materials, e.g. sandstones (TenCate 2011) and concrete (Scalerandi et al. 2018), to buildings (Astorga et al. 2019) and seismic fault zones (Johnson and Jia 2005).

TenCate et al. (2000) perceives the log-time relaxation as due to the restoration of microscopic contacts inhibited by a smooth energy barriers spectrum. This theory was further elaborated by Lebedev and Ostrovsky (2014) aiming to link classical nonlinearity with hysteresis and slow dynamics. The proposed model includes elastic forces due to grain compressibility and adhesion forces on contact surfaces. The recovery relies on thermal motion leading to longer relaxation times. Introducing microscopic fluctuations, the model was further developed to obtain macroscopic relaxation (Lebedev 2023). Vakhnenko et al. (2004, 2005) introduced the elastic modulus as a function of the concentration of defects, whose equilibrium value varies with the stress, and argues that the rates of bond breaking and restoration between grains are different, which allows the defect concentration to increase under dynamic loading reproducing the decrease in resonant frequency (modulus) and hysteresis during dynamic testing. Also, Favrie et al. (2015) and Berjamin et al. (2018) separate fast effects due to nonlinearity from viscoelasticity and slow processes due to development of defects. The exponential evolution of the concentration of defects towards a stress-dependent equilibrium with a long relaxation time explains the decrease of the modulus under dynamic loading, while the oscillations and hysteresis are described using a nonlinear form of the stress–strain relation. Attempts have also been recently made to link the observed phenomenology to mechanistic models, aiming to model coupling of non-equilibrium and classical nonlinearity (Remillieux et al. 2017) or the response to a dynamic forcing (Ostrovsky et al. 2019). It is often considered that redistribution of fluids is a significant contributing mechanism (Bittner and Popovics 2021), as the adhesive hysteresis of soft contacts possibly originates from surface roughness and viscoelasticity (Pérez-Ràfols et al. 2023). Since these models generally fail in predicting the observed log-time recovery during relaxation, a different approach was introduced, based on considering a distribution of features with different relaxation times. A multirelaxation model with a uniform distribution of relaxation times τ with lower and upper bounds is proposed by Snieder et al. (2017) to describe the log-time relaxation and justified by the Arrhenius law for energy of activation. Sens-Schönfelder et al. (2018) note that a broad distribution of relaxation times allows for the explanation of hysteresis and the formation of conditioning loops during harmonic excitation that arise from a combination of relaxation dynamics and an additional strain-dependent modulus variation.

Here, we present a time-delay model based on the concept of non-equilibrium strain proposed in Kober et al. (2023b). The model employs a wide range of relaxation times, which enable to accurately reproduce both elastic hysteresis and relaxation times spectra measured in experiments (Shokouhi et al. 2017). The fast and slow responses stem from the same equations, thus the model contains the experimentally observed influence of slow dynamics in fast dynamic experiments, both for what concerns the asymmetry of resonance curves at high amplitudes of excitation (TenCate and Shankland 1996) and the observed dependence of measured nonlinear elastic parameters on the experiment time scales (Scalerandi et al. 2020). Furthermore, previous models of elastic hysteresis (Van Den Abeele et al. 2001), could be considered as special cases of our model.

In Sect. 2, we give an overview of the features observed experimentally using a dynamic acoustoelastic testing (DAET) that should be described by the proposed model. The model of the non-equilibrium strain is introduced (Sect. 3) and an analytical solution for the harmonic loading case is presented and used to discuss the model properties. In Sect. 4, we show a few model predictions for common experimental protocols to demonstrate the potential for understanding of experimental observations. Lastly, in

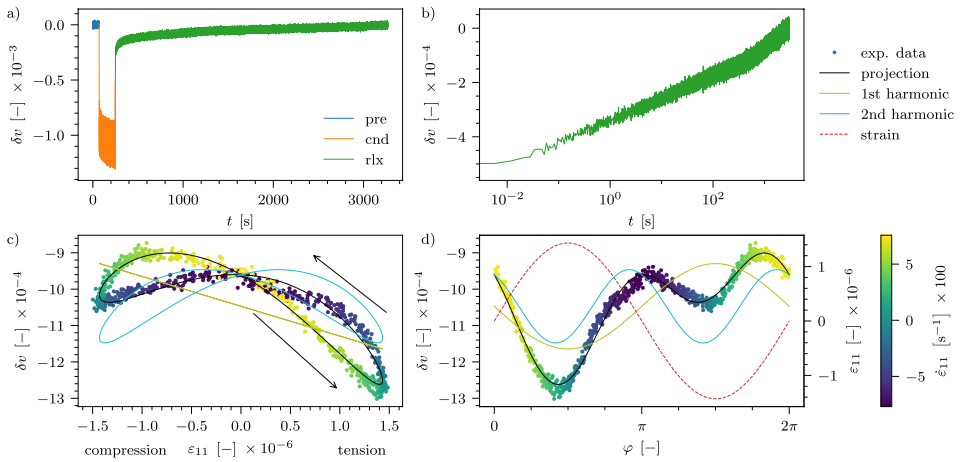

Fig. 1 Slow dynamics in the DAET experiment. **a** Relative velocity variation versus time during preconditioning (blue), conditioning (orange) and relaxation (green). **b** Relaxation: relative velocity variation versus log time. **c**, **d** Conditioning phase: relative velocity variation versus strain and strain phase. A color scale was used for the experimental datapoints to indicate branches of increasing (yellow) and decreasing (blue) strain at the moment of acquisition. A projection using the fundamental and second harmonic components is shown to fit the curve

Sect. 5, the model is validated by quantitative comparison with experimental data.

2 Slow and Fast Dynamics in Sandstones

2.1 Experimental Observations

The experimental data presented in this section show the typical elastic response observed in consolidated granular media. The data were collected using a dynamic acoustoelastic testing setup (DAET, see Appendix 1 for a detailed description of the experiment). The measurements were performed on a prismatic sandstone specimen excited near the first longitudinal resonance. Shear pulses propagating in the transverse direction were used to probe the velocity variations during conditioning and relaxation. The experiment thus allows assessing the variation dependence on both conditioning strain and time. The relative velocity variation δv is defined as

$$\delta v = \frac{v - v_0}{v_0}, \tag{1}$$

where v_0 is the unperturbed, linear velocity.

The experimental protocol consists of preconditioning, conditioning, and relaxation parts. In the preconditioning phase lasting 60 s, there is no dynamic excitation, and velocity remains constant at $v = v_0$ (see Fig. 1a, blue). The conditioning phase consists of high amplitude harmonic excitation at a frequency close to the first longitudinal mode for a duration of 180 s. Velocity (and hence modulus) oscillates (following the strain oscillation) around a negative "offset" value, which gradually decreases towards a non-equilibrium steady state, i.e. softening occurs (Fig. 1a, orange). When close to the steady state (i.e. 200 s $< t <$ 240 s), velocity variations can also be plotted as a function of the time-dependent conditioning strain (i.e. following the oscillations of velocity within one wave period). Higher harmonic oscillations are observed and hysteretic loops appear as shown in Fig. 1c. The end of the conditioning excitation is followed by a short (10 ms) ringdown after which no further excitation is performed for another 50 min. The relaxation phase (Fig. 1a, b, green) sees a slow recovery of velocity to its original value, i.e. the conditioning effect is fully reversible.

2.2 Harmonic Projection of Conditioning

During conditioning, the velocity oscillates due to the harmonic loading. When plotting the velocity variation as a function of the applied strain ε_{11}, closed loops appear (Fig. 1c) when conditioning time is sufficiently long. The curves can be decomposed into a series of harmonic components (i.e. the frequency of the harmonic excitation and its multiples) and analyzed using a projection procedure proposed by Rivière et al. (2013) for processing of DAET data. As it can be seen from the results of the projection in Fig. 1c, d, the fundamental and the second harmonic frequencies are the dominant components.

The fundamental harmonic component is due to classical nonlinearity as $\delta v = \beta \varepsilon_{11}$. The opposite phase with respect to the strain is caused by a negative coefficient β. While the fundamental results in a tilt in the closed loop, the higher harmonic components produce different values for branches

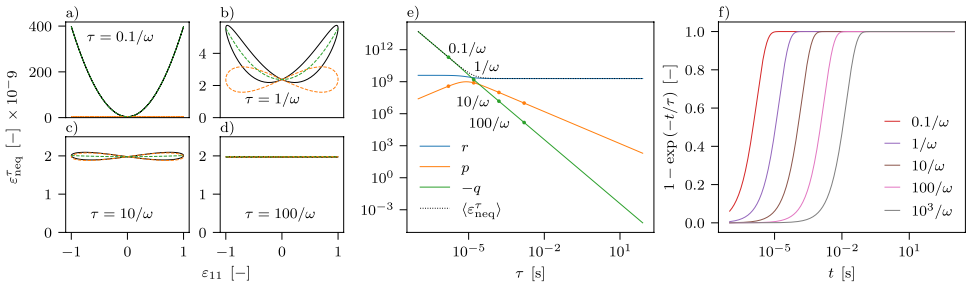

Fig. 2 Contributions of non-equilibrium strain components with different relaxation times to the loops and conditioning curves. **a–d** Loops corresponding to different relaxation times and their quadratic (green) and hysteretic (orange) components. **e** Offset and harmonic coefficients versus τ. Dots correspond to the relaxation times in subplots **a–d**. **f** Conditioning curves (i.e., offset vs. time) for different τ. Note that a $\log t$ scale is used. Data correspond to $f = 10\,\mathrm{kHz}$, $A = 1$, $\lambda = 1\mathrm{s}^2$

of increasing and decreasing strain, i.e. hysteresis. The shape of the hysteresis loop (Fig. 1d) is given by the phase shift of the second harmonic component with respect to strain.

2.3 Multirelaxation Theory

The evolution of velocity during relaxation (Fig. 1b) does not follow a log-time curve in the full time range. To account for the initial and final bending of the curve, a multirelaxation description (Shokouhi et al. 2017) is more appropriate. Such phenomenological approach describes the relaxation curve as a superposition of exponential decays with relaxation times τ weighted by a distribution $F(\tau)$,

$$\delta v(t) = \int_0^{+\infty} F(\tau) \exp\left(-\frac{t}{\tau}\right) \mathrm{d}\tau. \tag{2}$$

It has been shown that the distribution of relaxation times is challenging to derive from experimental data (Kober et al. 2023a). However, the functional form is not critical, since only a few properties of the distribution (mainly the position of the maximum and the asymmetry) determine the relaxation curve. A descriptive choice for fitting the relaxation curve is a generalized Weibull distribution (Kober et al. 2021),

$$F(\tau) \sim \left(\frac{\tau}{a}\right)^{b} \exp\left[-\left(\frac{\tau}{a}\right)^{c}\right], \tag{3}$$

with a positive scale parameter a and negative shape parameters b and c.

3 Non-equilibrium Strain Theory

In this section, we introduce a model of the non-equilibrium strain based on the phenomenological observations discussed in the previous section. In particular, we introduce a differential equation describing the evolution of the non-equilibrium strain, based on a multirelaxation scheme (Eq. 2) and accounting for the second harmonic component observed during conditioning.

3.1 Concept of Non-equilibrium Strain

The concept of non-equilibrium strain is based on the observation that the velocity variations are anisotropic and correlated even though the material is isotropic. The same correlation factors were measured in the case of quasi-static testing, conditioning and relaxation, which led to the introduction of the non-equilibrium strain into the classical acoustoelastic theory (Kober et al. 2023b),

$$\delta v_{ij} = \beta_{ij}\left(\varepsilon_{11} + \varepsilon_{\mathrm{neq}}\right). \tag{4}$$

Here, the indices i and j refer to the wave propagation direction and its polarisation. The non-equilibrium strain introduced above is a generic state variable, whose physical interpretation has to be ascribed to mechanisms, which are not discussed here. It is however sufficiently general to account for effects due to bond breaking, friction or water redistribution, which are commonly seen as possible sources of elastic hysteresis in the literature.

In our experiments, we consider shear velocities measured using pulses propagating in orthogonal direction and polarised parallel to the conditioning strain ($i = 2$, $j = 1$). Indices will be omitted in the following. Note also, that similar considerations apply for damping (Zeman et al. 2024). In Eq. 4, the total strain, in analogy with plasticity theories, is defined as a sum of applied elastic strain and the non-equilibrium strain. β_{ij} is the classical acoustoelastic coefficient. Note that the quadratic acoustoelastic term is neglected here, as it is unlikely to make a significant contribution to the observed velocity variation in the strain range considered here (as also applied by Sens-Schönfelder et al. 2018).

The non-equilibrium strain builds up when the material is subjected to strain (conditioning) and slowly disappears

when the strain is removed (relaxation). In accordance to the multirelaxation theory, we define the non-equilibrium strain to be a superposition of components $\varepsilon^{\tau}_{\mathrm{neq}}$ with relaxation times τ weighted by a distribution $\Psi(\tau)$,

$$\varepsilon_{\mathrm{neq}} = \int_0^{+\infty} \Psi(\tau)\varepsilon^{\tau}_{\mathrm{neq}}\mathrm{d}\tau. \tag{5}$$

We will discuss the link between the distribution $\Psi(\tau)$ and that derived analyzing experimental relaxation data ($F(\tau)$ in Eq. 2) in Sect. 4.

3.2 Evolution of Non-equilibrium Strain Components

The evolution of each component $\varepsilon^{\tau}_{\mathrm{neq}}$ is independent and given by a differential equation consisting of a conditioning term, here represented by a function f, and a relaxation term:

$$\dot{\varepsilon}^{\tau}_{\mathrm{neq}} = f(\tau, \varepsilon, \dot{\varepsilon}, \ldots) - \frac{1}{\tau}\varepsilon^{\tau}_{\mathrm{neq}} \tag{6}$$

In the absence of direct evidence for the physical sources of conditioning, we limit ourselves to introducing a phenomenological term, which satisfies the requirements imposed by available experimental observations (noting that the proposed definition is not necessarily unique or optimal). The observed phenomenology requires that:

- The accumulated non-equilibrium strain is positive as the velocity decreases due to slow dynamics, even in the case of harmonic loading. This requires f to be non-negative.
- For harmonic excitation, the non-equilibrium strain oscillates with a second harmonic frequency (see Sect. 2.2). This is achieved if f is an even function of a strain-related quantity.
- A specific phase of the strain quantity is necessary to obtain the hysteresis loop of the correct shape and orientation.

Based on the requirements above, we propose $f(\tau, \varepsilon, \dot{\varepsilon}) = \lambda(\varepsilon + \tau\dot{\varepsilon})^2/\tau^3$. The τ-dependent combination of strain and strain rate fulfills the phase condition (for a detailed analysis see Appendix 3). The normalization factor $1/\tau^3$ is chosen to guarantee that each $\varepsilon^{\tau}_{\mathrm{neq}}$ component contributes to the conditioning offset almost equally. The conditioning function contains a single scaling material parameter $\lambda > 0$.

The resulting model equation becomes

$$\dot{\varepsilon}^{\tau}_{\mathrm{neq}} = \frac{\lambda}{\tau^3}(\varepsilon + \tau\dot{\varepsilon})^2 - \frac{1}{\tau}\varepsilon^{\tau}_{\mathrm{neq}}. \tag{7}$$

Equation 7, together with Eqs. 4 and 5, allows to obtain the relative velocity variation vs. time as a function of any arbitrary conditioning excitation $\varepsilon(t)$. Relaxation is also described by the same set of equations, assuming $\varepsilon(t) = 0$.

3.3 Analytical Solution for Harmonic Excitation

Let us assume a harmonic excitation with frequency ω and amplitude A: $\varepsilon(t) = A\sin\omega t$. We also assume a fully relaxed initial condition, i.e. $\varepsilon^{\tau}_{\mathrm{neq}}(t = 0) = 0$. In this case, we can analytically solve Eq. 7 as:

$$\varepsilon^{\tau}_{\mathrm{neq}}(t) = r\left(1 - \exp\left(-\frac{t}{\tau}\right)\right) + q(\cos 2\omega t - 1) + p\sin 2\omega t. \tag{8}$$

The solution includes an offset term and two second harmonic terms. The offset term describes exponential accumulation of non-equilibrium strain in time with scaling coefficient r, i.e. r has the meaning of the asymptotic offset for infinite duration of conditioning. The second harmonic terms account for the properties of the conditioning loop (see Fig. 1). Specifically, p is the hysteretic coefficient (i.e. the vertical opening of the loop), q is the quadratic coefficient (i.e. the parabolic bending of the loop). The three coefficients p, q, r depend on the conditioning amplitude and frequency and vary with relaxation time τ as

$$\begin{aligned} r &= \lambda A^2 \frac{\omega^2 + 2\omega^4\tau^2}{1 + 4\omega^2\tau^2}, \quad p = \lambda A^2 \frac{\omega^3\tau}{1 + 4\omega^2\tau^2}, \\ q &= -\lambda A^2 \frac{1 + 3\tau^2\omega^2}{2\tau^2\left(1 + 4\omega^2\tau^2\right)}. \end{aligned} \tag{9}$$

Note, that the asymptotic offset r does not depend on τ when $\omega\tau \gg 1$. This allows the model to be consistent with the multirelaxation theory (Eq. 2), based on the superposition of components with equal contribution to the offset, weighted only by the distribution function. Also note $r \sim A^2\omega^2$, i.e. a quadratic dependency of the asymptotic offset on amplitude and frequency is intrinsic for this model.

Using Eq. 5, the total non-equilibrium strain can be expressed in the same form as Eq. 8,

$$\varepsilon_{\mathrm{neq}}(t) = R(t) + Q(\cos 2\omega t - 1) + P\sin 2\omega t, \tag{10}$$

where

$$\begin{aligned} P &= \int_0^{+\infty} \Psi(\tau)p(\tau)\mathrm{d}\tau, \quad Q = \int_0^{+\infty} \Psi(\tau)q(\tau)\mathrm{d}\tau, \\ R(t) &= \int_0^{+\infty} \Psi(\tau)r(\tau)\left(1 - \exp\left(-\frac{t}{\tau}\right)\right)\mathrm{d}\tau. \end{aligned} \tag{11}$$

The quantities P, Q and R have the meaning of the total hysteretic component, quadratic component and offset respectively. Note, that the P, Q coefficients are time-independent.

Thus the shape of the loop is constant during conditioning, while the total offset R evolves with conditioning time.

3.4 Contribution of Different Time Scales

As mentioned, each non-equilibrium strain component contributes to the properties of the total non-equilibrium strain in different ways depending on its relaxation time. The τ -dependence of the hysteretic coefficient p, quadratic coefficient q and the asymptotic offset r is discussed in Fig. 2 together with typical examples of resulting $\varepsilon^{\tau}_{\mathrm{neq}}$ responses. We remind that the loops and conditioning/relaxation curves in this section are upside down compared to Fig. 1, since positive non-equilibrium strain corresponds to negative velocity variations ($\beta < 0$).

Non-equilibrium strain components corresponding to "fast" relaxation times $\left(\tau \ll \omega^{-1}\right)$ are mostly driven by the ε^2 term in Eq. 7. Therefore, the coefficient q of the quadratic term in Eq. 8 is dominant by orders of magnitude, leading to a predominantly quadratic loops (Fig. 2a). With increasing τ the effect of $\dot{\varepsilon}$ becomes more and more important in introducing a phase shift, i.e. increasing the hysteretic contribution. For "moderate" relaxation times $\left(\tau \sim \omega^{-1}\right)$, the quadratic and hysteretic coefficients are of the same orders of magnitude (Fig. 2b, c). In the range of "slow" relaxation times $\left(\tau \gg \omega^{-1}\right)$ only the offset is significant (Fig. 2d), while the contribution to the loop shape is negligible.

3.5 Distribution of Non-equilibrium Strain

In order to evaluate the total non-equilibrium strain from its components, the last feature to be defined is the distribution $\Psi(\tau)$. Currently, there is an absence of experimental evidence regarding the form of the distribution. Given the properties of the harmonic solution Eq. 9, it can be deduced that $\Psi(\tau)$ must decay to zero fast enough for both $\tau \to 0$ and $\tau \to \infty$ to compensate the divergence of p and r in Fig. 2e.

For simplicity and in analogy with choices reported elsewhere (Snieder et al. 2017; Sens-Schönfelder et al. 2018), we define the distribution in the form

$$\Psi(\tau) = \frac{1}{\tau}, \quad \tau_{\min} < \tau < \tau_{\max}, \tag{12}$$

which leads in conjunction with exponential relaxation functions to a log-time process, as shown by Snieder et al. (2017). Both lower and upper bounds ($\tau_{\min}$ and $\tau_{\max}$) of the distribution are necessary for integrability (finite non-equilibrium strain). Note that this distribution can also be seen as a uniform distribution of logarithms of relaxation times. Following the transformation theorem, $\Psi(\tau)$ is equivalent to $\widetilde{\Psi}(\log \tau) = \tau\Psi(\tau) = 1$.

All following results presented in $\log \tau$ scale are plotted as transformed distributions $\widetilde{\Psi}$, since they unmisleadingly represent the weights of different time scales.

4 Numerical Results

The properties of the harmonic solution given above are shown calculating the model predictions for several numerical experiments, which reproduce some common experimental procedures. The first aim is to explain the relation between the distribution of non-equilibrium strain $\Psi(\tau)$ and the distribution of relaxation times $F(\tau)$ from the multirelaxation theory in Eq. 2. The second aim is to show the origin and properties of cumulative conditioning. In both cases, the temporal evolution of the offset only is relevant, since the harmonic content of $\varepsilon_{\mathrm{neq}}$ does not evolve in time.

4.1 Finite Conditioning and Relaxation Spectrum

Let us assume an experimental protocol as illustrated in Fig. 1a: a specimen is conditioned using external harmonic loading for a finite period T_{cnd} and then a relaxation is measured. The conditioning spectrum, i.e. the Ψ-weighted set of non-equilibrium strain offset, will evolve in time as

$$S_{T_{\mathrm{cnd}}}(\tau) = \Psi(\tau) r(\tau) \left[1 - \exp\left(-\frac{T_{\mathrm{cnd}}}{\tau}\right)\right]. \tag{13}$$

The components are induced gradually depending on their relaxation time. As it can be seen in Fig. 3a, the contribution to the offset of slow relaxation times, $\tau \gg T_{\mathrm{cnd}}$, is limited. In other words, the spectrum inducible by finite-duration conditioning is limited by the conditioning duration.

After the conditioning period, the loading is turned off and relaxation phase begins. A major part of the non-equilibrium strain relaxes within a fraction of a second and is hardly measurable due to limited probing rate of the equipment available for experiments. Furthermore, the strain does not disappear instantaneously when conditioning is switched off, but a ringdown occurs, delaying the probing of relaxation as well. Let us suppose a short time gap T_0 between switching the conditioning off and the first measurement of the relaxation. After this period, the non-equilibrium strain components of fast relaxation times are gone and the spectrum is already modified as $S_{T_{\mathrm{cnd}}}(\tau) \exp\left(-\frac{T_0}{\tau}\right)$. The ringdown effects, in conjunction with an ambiguous definition of the beginning of the relaxation phase, result in the behavior observed at the earliest times of slow dynamic recovery examined by Lee and Weaver (2024).

To summarize, we start with an approximately uniform distribution of non-equilibrium strain (in $\log \tau$), which is equivalent to the asymptotic conditioning spectrum $S_{\infty}(\tau)$

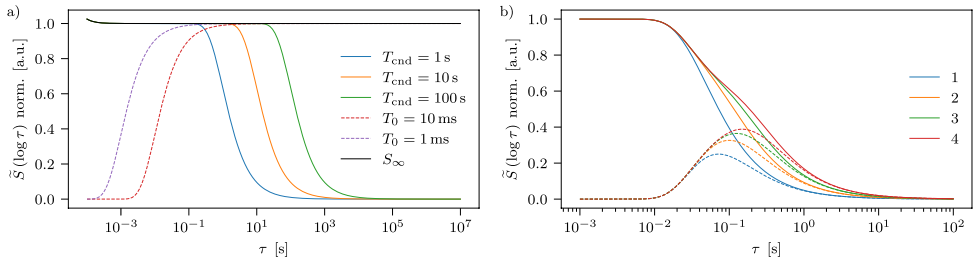

Fig. 3 Spectrum of the non-equilibrium strain. **a** Spectra induced by conditionings of different durations (solid lines) and partially relaxed spectra (dashed lines) for different ringdown duration and $T_{cnd} = \infty$. Note that the partially relaxed spectra overlap almost perfectly with the conditioning branch at large τ. Plots are obtained using the cut-off and window functions introduced in the text. **b** Spectra after repeated conditionings (solid lines) and relaxations (dashed), showing cumulative effects. Here, we choose $T_{cnd} = 50$ ms, $T_{rlx} = 50$ ms. Normalized distributions of logarithms of relaxation times are shown, upper and lower bounds of $\Psi(\tau)$ are not considered

(i.e. the spectrum induced by an infinite conditioning). This spectrum is only bounded by τ_{min} and τ_{max} related to the distribution Ψ. The conditioning spectrum in practical experiments is further limited by a "cut-off" function for $\tau > T_{cnd}$ and the relaxation spectrum is further curbed for $\tau < T_0$. The resulting relaxation spectrum (corresponding to that reported in multirelaxation theory in Eq. 2) is then $F(\tau) = W(\tau)S_\infty(\tau)$, where the window function $W(\tau)$ cuts off the relaxation times too fast to be measured and too slow to be induced. Fig. 3a illustrates the spectra induced by finite conditionings of different durations and relaxation spectra after a short time gap.

Let us remark that the proposed model predicts an effective distribution consistent with the parametric distribution used for fitting relaxation data (Kober et al. 2021): the underlying distribution multiplied by the relaxation term $\frac{1}{\tau}\exp\left(-\frac{T_0}{\tau}\right)$ is a case of the generalized Weibull distribution (Eq. 3).

4.2 Cumulative Conditioning Effect

The proposed model is linear in ε^τ_{neq}, which means that individual conditionings and following relaxations can be considered independently and summed. Moreover, relaxation of each component of the non-equilibrium strain is an exponential and thus infinite process. These two premises result in the following expected behavior: when a conditioning induced a non-equilibrium strain in a specimen, which is partially relaxed and conditioned again, the non-equilibrium strain includes a part generated during the last conditioning as well as a residual part generated during the preceding conditioning.

We can write the solution for arbitrary initial conditions as a superposition of relaxation from the initial state and an independent conditioning from a fully relaxed state:

$$\varepsilon^\tau_{neq}(t) = \varepsilon^\tau_{neq,cnd}(t) + \varepsilon^\tau_{neq,rlx}(t), \tag{14}$$

where the first term follows Eq. 8 and the second term relaxes from the initial value $\varepsilon^\tau_{neq}(0)$ as

$$\varepsilon^\tau_{neq,rlx}(t) = \varepsilon^\tau_{neq}(0)\exp\left(-\frac{t}{\tau}\right). \tag{15}$$

Let us now assume repeated conditionings with a harmonic excitation at a constant amplitude and duration T_{cnd}, interleaved by relaxations of duration T_{rlx}. In Fig. 3b, the spectrum after nth conditioning and nth relaxation is illustrated. Only the highest relaxation times partially persist after relaxations, and their cumulation makes the right tail of the spectrum heavier after successive repetitions of conditioning.

Cumulative conditioning effects predicted by the model are consistent with experimental observations. In experiments, conditioning phases (excitation on for a finite duration) are always interleaved with relaxation phases (a short time interval during which excitation is off, e.g. to allow to change frequency or amplitude). The conditioning and relaxation times T_{cnd} and T_{rlx} used here, have been chosen to be consistent with typical timing of NRUS probing, in which a significant role of cumulative conditioning was observed by Kober et al. (2025)

5 Model Validation on Experimental Data

In this section, the proposed model is validated by comparing quantitatively the model results with experimental data obtained using dynamic acoustoelastic testing. DAET data are collected for several amplitudes of conditioning and a repeated set of measurements is performed to assure experimental consistency. Based on the best fitting of the experimental data, model parameters are derived.

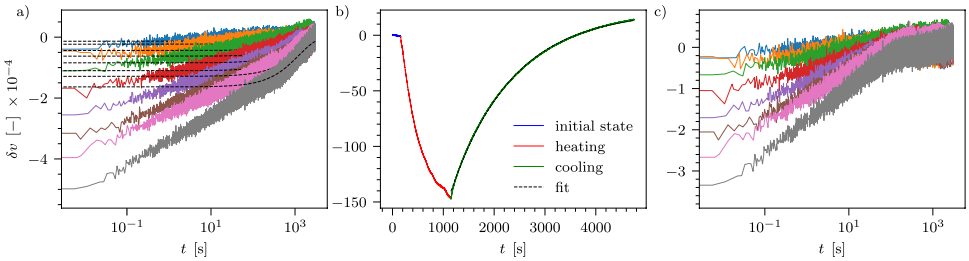

Fig. 4 Relaxation curves and temperature correction. **a** Relaxation curves for different conditioning amplitudes and temperature components obtained by fitting the later times (dashed black curves). **b** Velocity variation during heating experiment with exponential fit of the cooling phase. **c** Relaxation curves with the temperature contribution removed.

5.1 Experimental Observations

As already discussed in Sect. 2, in dynamic acoustoelastic testing, velocity variation can be measured in the transverse direction of the sample using propagating pulses (high frequency probe). Measurements are taken at successive times both while the sample is conditioning (a pump harmonic excitation is applied in the longitudinal direction of the sample) or relaxing (when the pump is off). As a result, velocity evolves with time and typical results are given in Fig. 1a. More details about the experiment can be found in Appendix 1.

5.2 Heat Exchange Correction

Before proceeding with fitting using the model, experimental data have been processed to remove any effect, which could have contaminated the measurement and are not related to the conditioning process we wish to describe with our model. In particular, we have focused on the relaxation phase, since this phase was more frequently studied in the literature, thus allowing some reference of the expected quantitative behavior. The temporal evolution of velocity variation during relaxation after increasing amplitudes of the conditioning strain is reported in Fig. 4a.

For each conditioning amplitude two distinct sections of different slopes of the relaxation curves are present as the relaxation speeds up at about 1000 s. This behavior corresponds to a bimodal distribution of relaxation times. We suggest the secondary peak to be caused by temperature effects due to heat generation during the conditioning phase. To test the hypothesis, an auxiliary heat exchange experiment was performed during which velocity was probed. The sample was heated externally and once the heat source was removed, an exponential cooling was observed (Fig. 4b). Despite the differences between the heating experiment and DAET conditioning, the heat exchange rate approximates well the slow process observed in DAET.

Velocity variations due to the cooling effect must be removed from the data. To this purpose, we fit the later times of the relaxation curves $\left(t > 1 \times 10^3 \text{ s}\right)$ with the cooling phase exponential (black dashed line in Fig. 4b) and subtract it from the data in the full time range, resulting in the plots reported in Fig. 4c. A correction must also be applied to data in the conditioning phase, for which only subtracting a constant term from the offset is needed. In the following, we report already corrected experimental data.

5.3 Model Fitting Procedure

The model validation requires fitting model parameters, which are material properties, while considering experimental procedure as well. The material properties include: the classical nonlinear parameter β, the lower and upper bounds of the distribution of relaxation times τ_{min} and τ_{max}, and the conditioning coefficient λ. These will be estimated by fitting conditioning loops. In the following analysis, it was assumed that the upper bound of relaxation time distribution was not reached, i.e. $\tau_{\text{max}} \gg T_{\text{cnd}}$, and therefore, the limiting factor for high τ components stems only from the conditioning duration.

Other quantities are predetermined and experiment related. They are the strain amplitudes, the conditioning duration $T_{\text{cnd}} = 180\,\text{s}$, the ringdown time $T_0 = 10\,\text{ms}$ and the rate of the exponential decay $640\,\text{s}^{-1}$. The latter are the same for all amplitudes and are only relevant for the determination of relaxation spectra.

5.4 Conditioning

In the conditioning phase, we focus on the conditioning loops rather than on the evolution of the offset, as they carry information about the complete range of relaxation times. We fit the experimental data using only three model parameters: β, the lower bound of the distribution of relaxation times τ_{min}, and the conditioning coefficient λ. The confidence interval for the parameters estimation defines a very low error on parameters (e.g. about one per thousand for the log of τ_{min}).

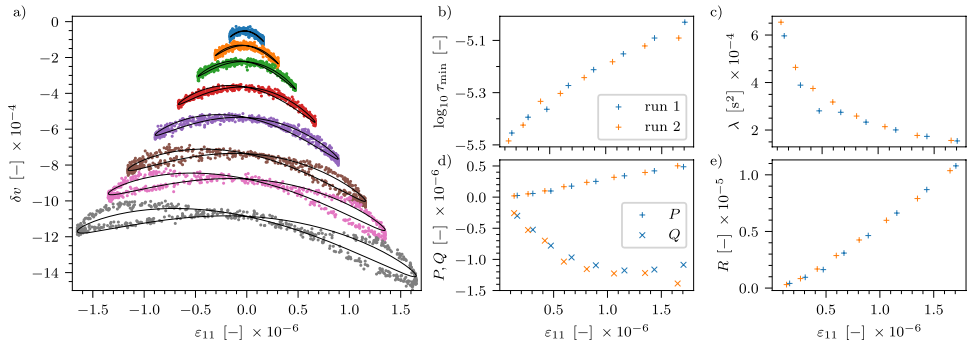

Fig. 5 Conditioning loops. **a** Experimental data for different amplitudes and fit of the model. **b–e** Model parameters τ_{min} and λ versus conditioning strain. Loop components coefficients P, Q and offset R. Two repetitions of the experiment were performed, demonstrating the repeatability of the procedure

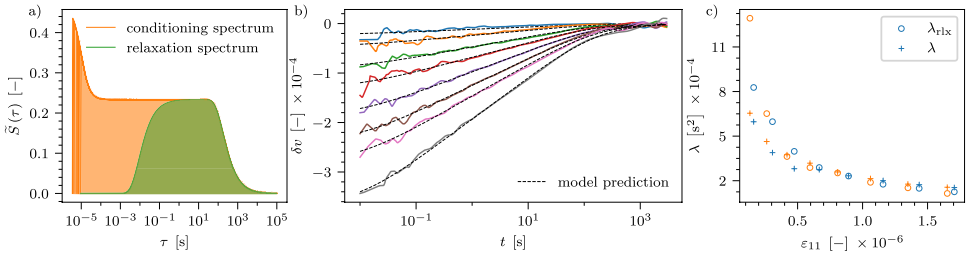

Fig. 6 **a** Spectra of the non-equilibrium strain at the end of conditioning (for different amplitudes, normalized) and after the ringdown. Note that we plot the distribution of $\log \tau$ here. **b** Relaxation curves for different conditioning amplitudes with the model prediction. Solid lines are experimental data from Fig. 4c resampled logarithmically using a kernel smoother/interpolator. **c** Comparison of conditioning coefficients λ estimated by fitting conditioning and relaxation data

The acoustoelastic coefficient β was determined by fitting the slope of the fundamental component and we obtained $\beta = -75$ as the optimal value for all amplitudes. The non-equilibrium strain parameters λ and τ_{min} are estimated for all amplitudes of conditioning independently. The results of the fit are shown in Fig. 5a; the estimated parameters are reported in Fig. 5b, c. The harmonic coefficients P, Q describing the loop are shown in Fig. 5d, e.

The model parameters (τ_{min} and λ) and hence the loop coefficients (P, Q, R) are observed to be amplitude dependent. The loops for low amplitudes are more quadratic, thus the corresponding range of relaxation times reaches smaller values, i.e. τ_{min} increases with amplitude. The lower bound of the distribution is critical as it controls the ratio of quadratic and hysteretic components of the conditioning loops. It allows to estimate τ_{min} from conditioning experimental data. We have estimated that $\tau_{min} \approx 1 \times 10^{-5}$s, i.e. the distribution contains much smaller relaxation times than what its estimation based on relaxation data would suggest. These findings will be further discussed in Sect. 6. For a comparison with fitting the data using the hysteretic model, see Appendix 4.

5.5 Relaxation

The main focus of model verification using relaxation data is to reproduce the temporal evolution using the distribution of non-equilibrium strain components derived in the conditioning phase. Indeed, fitting the conditioning phase, besides predicting the loops of velocity vs. strain (Fig. 5a), also allows to estimate the distribution of non-equilibrium strains at the end of conditioning (Fig. 6a). Note that conditioning spectra for all strain amplitudes share the upper limit given by T_{cnd} and differ slightly due to the amplitude dependent τ_{min}. On the contrary, the relaxation spectra for all conditioning amplitudes have the same shape and differ only in scale. This is due to the ringdown time T_0, which completely removes a significant portion of the low relaxation time components.

The resulting relaxation spectrum (equivalent to the spectrum $F(\tau)$ in the multirelaxation theory) is used to model the observed temporal evolution of velocity during relaxation. Results agree very well with the experimental data (Fig. 6b) for all conditioning amplitudes.

Furthermore, it is possible to estimate the conditioning coefficient λ from the scaling parameter of the relaxation curve fitting (given that the acoustoelastic constant β is known). This allows us to independently cross-validate the λ estimates based on conditioning and relaxation data. The comparison is shown in Fig. 6c. In the range of intermediate to high amplitudes, we have a good quantitative agreement (0.5 µstrain $< \varepsilon <$ 1.2 µstrain). Incidentally, this range corresponds to the amplitude range in which we obtain the best fitting of the conditioning loops. At lower

strains, the agreement is limited both for λ estimates and for conditioning loop fitting. The difference in case of low strain measurements is most likely due to noise. Considering the various limitations of the model and experimental uncertainties, which are discussed in the next section, the agreement between the estimated λ is good, even at large strains for which some discrepancies are also present.

6 Discussion

The main importance of the model is that it allows to define fast/slow dynamics and classical/non-classical effects in a comprehensive way. Some details of the model (namely the distribution $\Psi(\tau)$ and the choice of the conditioning term in Eq. 7) might be debatable but not crucial for many model predictions as will be discussed in this section.

The model describes fast and slow dynamic effects in the same way. The distinction between fast and slow concerns the range of relaxation times involved in each process. As the following definition suggests, these ranges can, to some extent, depend on excitation parameters:

- Fast dynamics is given by non-equilibrium strain contribution from low relaxation times components. These can reach full conditioning or relaxation within a single period of excitation. As such, they describe the part of measured data that is repeatable in time, or, in other words, that behaves in the same way independently from the duration of the experiment or experimental setup details. The range of low τ components responsible for fast dynamics may vary with respect to the applied conditioning wave period.
- Slow dynamics is produced by non-equilibrium strain contributions due to intermediate to large τ components. The relaxation of these components takes much longer than the conditioning phase that induced them. In cases of incomplete relaxation, cumulative effects are present leading to limited repeatability.

Some other features of the model must also be discussed. First of all, the model has an inherent quadratic dependence on the strain amplitude and frequency due to the quadratic conditioning function. This choice results in conditioning loops that are close to the experimental data in shape (see Fig. 5a), but not necessarily reproduce well the observed dependence of the offset (which is normally what is measured e.g. in nonlinear resonant ultrasound spectroscopy experiments). Contradictory data have been reported in the literature and both linear and quadratic amplitude dependencies were observed in sandstones (Kober et al. 2023b; Rivière et al. 2013). The model proposed allows to produce any dependence (which was mostly linear in our case, Fig. 5e) introducing amplitude dependent hysteretic parameters (λ and $\tau_{\min}$). Whether such amplitude dependence exists in the form of an actual physical mechanism or a modified conditioning function is needed, requires further investigation.

So far, the experimental data reported in the literature indicate that the conditioning function may be complex, e.g. with a quadratic behavior for low strains and linear for higher strains (Remillieux et al. 2016). Modifying the conditioning function in Eq. 7 (preserving the strain and strain rate combination) would lead to a modified amplitude and frequency dependence of the total non-equilibrium strain, but with appropriate parameters possibly not giving any distortion of the conditioning loops. More importantly, the conclusions on the contributions of different time scales would remain valid.

Related to the problem of determining the conditioning function, we also consider the measurement and approximation of strain as an issue to be clarified. The strain estimation (used both in this paper and others) is often based on the assumption of a linear, homogeneous material, while the properties of the material become inhomogeneous and anisotropic due to the slow dynamics behavior. Since the DAET measurement is localized in the area with maximal strain amplitude, the deviation from linear strain approximation could be significant and thus the strain dependence could be different than that normally reported.

Concerning the role of classical and non-classical terms, we remark that the model includes a wide range of time scales that, ordered by the relaxation times, are responsible for the quadratic shape of the conditioning loops, hysteretic component and evolution of the offset. We emphasize that the quadratic component resulting for our model is given by non-classical effects, unlike for other models that interpret it as an independent parameter of classical nonlinearity (Van Den Abeele et al. 2001). Recall that only the linear term of the classical nonlinearity is considered in this work (Eq. 4). In fact, in other experiments (Kober et al. 2023b), the quadratic classical nonlinear coefficient was measured during quasi-static loading (i.e. at larger strains) and the value obtained ($\delta \approx 4 \times 10^4$) makes it unrealistic that it could explain the quadratic component in the dynamic range used here.

Finally, concerning the choice of the distribution of relaxation times, we have assumed $\Psi(\tau) = 1/\tau$ in the range between $\tau_{\min}$ and $\tau_{\max}$. While it was possible to estimate the lower bound from conditioning data, the upper bound could not be estimated neither from the relaxation curves, because slow components cannot be induced by a finite-duration conditioning, hence are not contributing to the offset (see Sect. 4.1), nor from the conditioning loops, because the shape coefficients of the oscillating terms

rapidly decline with the relaxation time (see Sect. 3.4). The dependence of the relaxation spectrum on conditioning duration is consistent with experimental observations reported in (Lebedev and Manakov 2024). It is conceivable, that the distribution of relaxation times could be more complex. Certainly, adjustments to the distribution function would allow for a better fitting of the presented data. At the same time, the level of agreement of our observations with the current definition is notable.

It is important to note that the non-equilibrium strain model describes a local velocity change in the presence of external mechanical loading. It is not possible at this point to evaluate the feedback, i.e. the effect that the induced change of velocity has on the loading. E.g., in resonant experiments, the conditioning induces a shift of the resonance peak and consequently a change of the strain distribution in the sample. Such strain redistribution is likely why DAET experiments may present different shapes of the conditioning and relaxation curves. Li et al (2018) studied the resulting feedback proposing an approach which could be done also using our model. Furthermore, the model proposed assumes that the non-equilibrium strain components relax with the same rate as they were induced, thus the relaxation curves are approximately the conditioning curves turned upside down, transitioning from the corresponding level reached during conditioning to zero. This is in agreement with experimental observations showing a linear correlation between conditioning and relaxation curves in concrete samples (see e.g. Scalerandi et al. 2019).

7 Conclusions

In this work, we extended the concept of non-equilibrium strain, which has been proposed to describe the non-classical nonlinear behavior of consolidated granular materials. We developed a time-delay model to explain velocity variations in response to dynamic perturbations based on experimental observations obtained through dynamic acoustoelastic testing.

The model consists of a decomposition of the non-equilibrium strain into a wide spectrum of components that evolve independently with different rates (relaxation times) following a linear differential equation. We demonstrated that fast relaxation times are responsible for generation of the second harmonic component of the velocity variations in response to harmonic loading, i.e. causing hysteresis and cubic nonlinearity. At the same time, the slow relaxation times are involved in the gradual decrease in velocity during conditioning and its recovery during relaxation. This implies that although the distribution of relaxation times is broad, only a subset of it constitutes the relaxation spectrum, i.e. the distribution derived from relaxation curves obtained experimentally.

Our findings demonstrate that in order to accurately describe the nonlinear behavior in terms of strain, it is necessary to include a conditioning source that depends on both strain and strain rate to generate conditioning loops that are consistent with experimental observations. Furthermore, the model is compatible with previous modelling efforts proposed for DAET experiments and slow dynamics in general.

Some of the features of the model (e.g. the choice of the relaxation times distribution function and the choice of a quadratic conditioning term in the differential equations), still need to be discussed and perhaps modified. However, at the current stage, a realistic description of some of the model details is hindered by conflicting experimental observations reported in the literature and discussed measurement limitations.

Nevertheless, the main contributions of the model to the understanding of the phenomena responsible for hysteresis and conditioning in sandstones remain valid independently from the model details. As such, the model could be a useful tool to interpret experimental observations and/or simulate experiments in time/strain/frequency ranges that cannot be reached in real experiments, giving possibly useful insights about the physical mechanisms originating non-classical elasticity.

Appendix 1: Experimental Setup of DAET

Experimental data are obtained using the dynamic acoustoelastic testing setup illustrated in Fig. 7. The measurements are performed on a prismatic sample of Czech sandstone of a square cross-section with a transverse dimension of 25 mm and length of 140 mm. The sample is suspended horizontally in order to obtain free boundary conditions, and placed in a styrofoam box in order to reduce environmental effects due to humidity and temperature variations.

The sample is equipped with a pair of low-frequency PZT disks (APC 20 × 2 mm rings) and a pair of high-frequency shear wave transducers (Olympus V154) glued using a thermoplastic monomer (Crystalbond 555). One transducer of each pair is used as an acoustic source and one is a receiver. PZT disks, attached on the bases, are used for exciting the sample and measuring in the longitudinal direction. Sinusoidal loading is used to excite the first compressional mode (8.4 kHz), the resonant frequency was preliminarily estimated using low-amplitude chirp excitation.

Shear transducers, attached in the centres of opposite sides of the sample, are measuring in the transverse direction. Short pulses (one period of 1 MHz sine signal) are being transmitted and received allowing to monitor

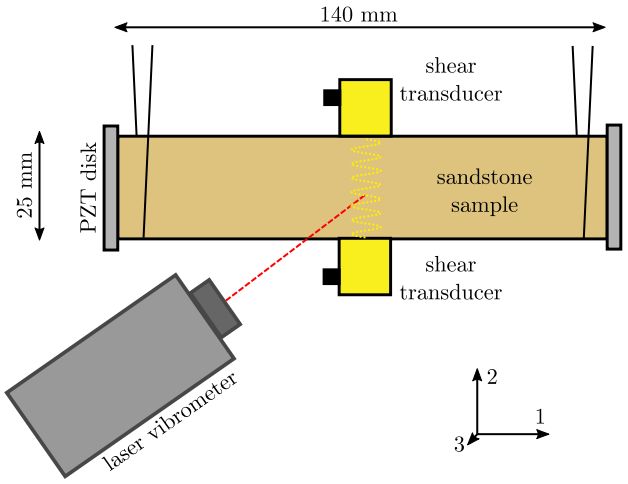

Fig. 7 Experimental setup for the DAET experiment

relative velocity variation using time-of-flight variations ΔTOF obtained using cross-correlation with a reference pulse (measured before conditioning) and propagation distance d as

$$\delta v = \frac{\Delta \mathrm{ToF}}{d} v_0, \tag{16}$$

where $v_0 \approx 2600\,\mathrm{ms}^{-1}$ is the linear velocity (measured without any induced strain). The shear waves are polarized parallel with respect to the longitudinal direction, i.e., measuring relative velocity variation δv_{21}. The pulse amplitude is small in order to have linear propagation in a medium with elastic properties perturbed by the conditioning phase. The repetition rate of the pulse transmission (and thus sampling of the velocity variations) is roughly 100 Hz.

A laser vibrometer (Polytec OFV-505 with OFV-5000 controller) is measuring the normal velocity of the surface in the centre of the sample. The velocity is then converted into strain in the longitudinal direction $\left(\varepsilon_{11}\right)$. The phase of the strain estimation is affected by the apparatus latency and a correction based on the phase of the velocity variations (fundamental component, classical nonlinearity) is applied.

The transducers and vibrometers are connected to Keysight/Signadyne M3300A arbitrary waveform generator and oscilloscope. A power amplifier (Tabor 9400) is used for the transmitting PZT disk. The shear wave receiver is connected via a preamplifier (Mistras 2/4/6, 40 dB) adjusting the pulse amplitudes and filtering out the low frequency signal due to excitation. The high-frequency pulses are sampled by 100 MHz and the low-frequency channels are sampled by 1 MHz.

The experimental protocol consists of a short preconditioning measurement (60 s), conditioning (180 s) and relaxation (3000 s). The preconditioning phase provides signal references used for the estimation of velocity variations. During conditioning, the PZT disk injects a sinusoidal signal on the selected conditioning amplitude exciting the first compressional mode. The procedure was repeated twice for each conditioning amplitude (output voltage 0.4 V to 1.8 V in steps of 0.2 V) leaving adequate pauses between repetitions to ensure full relaxation.

Appendix 2: Heating Experiment

In the heating experiment, a heating plate (VELP Scientifica REC 7) was brought up to the temperature of 55 °C and placed under the sample suspended in the same position as in the DAET experiment, the gap between the heater and the sample was approximately 1 cm. After 15 min, the heater was turned off and removed. Velocity variation was measured during the heating and following cooling.

A significant drop in the velocity was observed (Fig. 4b) followed by an exponential recovery. Fitting the cooling phase with $a \exp(-t/\tau)$, a "relaxation time" $\tau = 1221$ s corresponding to the heat exchange rate was obtained. The results support our hypothesis that the high-amplitude harmonic loading causes heating of the sample either due to heat generation in the piezoelectric actuators or in the vibrating sample itself. When the conditioning is turned off, the sample is cooling exponentially to the ambient temperature by a heat exchange with the air.

Appendix 3: Conditioning Loops: Shape and Orientation

The closed curves in Figs. 1 and 2 are formed as the quantity on x-axis (strain) oscillates as $x(t) \sim \sin \omega t$ and the quantity on y-axis (velocity variation or non-equilibrium strain) with double the frequency and phase shift, $y \sim \sin(2\omega t + \phi) = p \sin 2\omega t + q \cos 2\omega t$. The sine term forms a symmetrical self-intersecting closed curve, $y_1(x) = 2px\sqrt{1-x^2}\,\mathrm{sgn}\,\dot{x}$, where the sign of the coefficient p determines the orientation of the loop. The cosine term forms a parabola, $y_2(x) = q\left(1 - 2x^2\right)$. Coefficients of these terms are given by the phase ϕ.

Let us assume a differential equation for components of the non-equilibrium strain where the driving quantity is a sine function with an arbitrary phase shift φ (constant or τ-dependent) representing strain, strain rate or a combination of these quantities:

$$\dot{\varepsilon}^{\tau}_{\mathrm{neq}} = [\sin(\omega t + \varphi)]^2 - \frac{1}{\tau}\varepsilon^{\tau}_{\mathrm{neq}}. \tag{17}$$

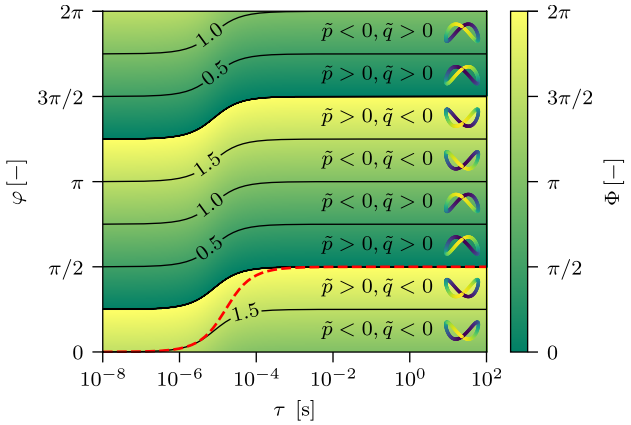

Fig. 8 Phase shift of the non-equilibrium strain components and shapes of the loops for different phase shift in the driving quantity. Phase shift corresponding to Eq. 7 (red dashed line). The colors of the loops are the same as in Fig. 1, i.e. increasing strain is yellow, decreasing strain is blue. Conditioning of frequency $f = 10\,\text{kHz}$ was used for this illustration

The equation is solved by

$$\begin{aligned}\varepsilon^{\tau}_{\text{neq}}(t) \sim& \tilde{r}\left(1-\exp\left(-\frac{t}{\tau}\right)\right) + \tilde{q}(\cos 2\omega t - 1) + \tilde{p}\sin 2\omega t \\ =& \tilde{r}\left(1-\exp\left(-\frac{t}{\tau}\right)\right) + \sqrt{\tilde{p}^2+\tilde{q}^2}\sin(2\omega t + \Phi),\end{aligned} \tag{18}$$

where

$$\begin{aligned}\tilde{p} &= \sin 2\varphi - 2\omega\tau\cos 2\varphi, \\ \tilde{q} &= -2\omega\tau\sin 2\varphi - \cos 2\varphi.\end{aligned} \tag{19}$$

Figure 8 illustrates how the phase shift Φ of the solution depends on the phase shift φ of the driving quantity and relaxation time τ. The loops are obtained by plotting the non-equilibrium strain as a function of strain (sine function with no phase shift). For each phase Φ, loops with different orientations and concavities are obtained, as shown in Fig. 8.

To obtain a loop with the shape observed experimentally, i.e. composed of an upward-facing parabola and a self-intersecting hysteresis loop, where velocity is higher during dynamic strain reduction than during strain increase ($\dot{\delta v} > 0$ at maximum tension, or vice versa in terms of non-equilibrium strain), $p > 0$ and $q < 0$ are required. These conditions are satisfied in the curved regions where $\Phi \in \left[\frac{3}{2}\pi, 2\pi\right]$.

The choice used in this paper for the conditioning term (Eq. 7) leads to $\varphi(\tau) = \arctan \omega\tau$ and satisfies these conditions for all relaxation times (dashed line in Fig. 8).

Appendix 4: Hysteretic Model

The model reported here is not contradicting the interpretation of DAET loops proposed by other authors and based on the hysteretic model. Indeed, our model is a generalization, including time dependence of conditioning of the hysteretic model, which can be used to fit data when an additional offset term is considered.

The generalized phenomenological hysteretic model can be written as

$$\delta v(\varepsilon(t)) = \beta\varepsilon + \delta\varepsilon^2 + \alpha(\Delta\varepsilon + \varepsilon\,\text{sgn}\,\dot{\varepsilon}) + o, \tag{20}$$

where the classical nonlinearity parameter $\beta = -75$ (same as in the Sect. 5.4) and parameters δ (quadratic term), α (hysteresis) and o (offset) are to be estimated by fitting experimental data. The results are presented in Fig. 9. All three parameters depend on conditioning amplitude.

The parameter δ, which is usually interpreted as a coefficient of classical nonlinearity (hence amplitude-independent material parameter) (Van Den Abeele et al. 2001), here exhibits strong dependence on conditioning amplitude. Also its values are different from its estimation using static acoustoelastic testing performed on the same material, $\delta \approx 10^4$, in Kober et al. (2023b). This indicates that δ in Eq. 20 is not the classical second order acoustoelastic parameter and the quadratic effect has a non-classical origin.

The solution obtained using our model for harmonic excitation can be expressed in terms of strain as

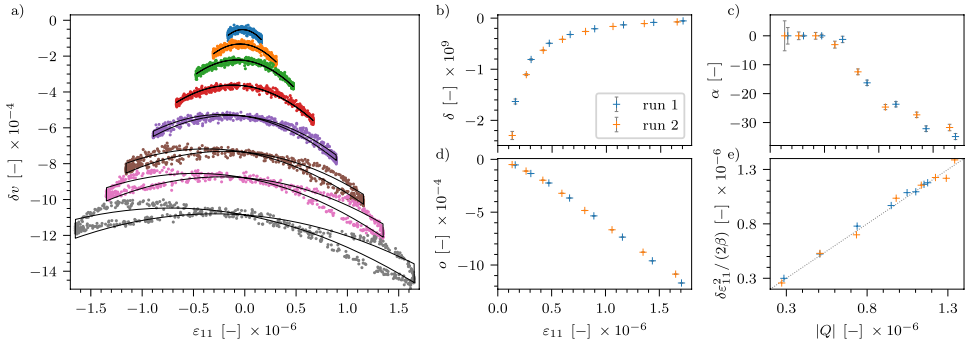

Fig. 9 Conditioning loops and hysteretic model. **a** Conditioning loops for different amplitudes and fit (same colors as in Fig. 5). **b–d** Model parameters δ, α and offset versus conditioning strain amplitude. **e** Correlation of parameters δ and Q (dotted line is identity)

$$\delta v(\varepsilon(t)) = \beta\varepsilon(t) + \beta R(t) - \frac{2\beta Q}{A^2}\varepsilon^2(t) + \frac{\beta P}{A^2}\varepsilon(t)\sqrt{A^2 - \varepsilon^2(t)}\,\mathrm{sgn}\,\dot{\varepsilon}, \tag{21}$$

i.e. both our model and the hysteretic model consist of linear, quadratic, hysteretic and offset terms and the loop coefficients and model parameters are correlated: $\delta \sim Q$, $\alpha \sim P$. Comparison of the solution of the proposed model and Eq. 20 implies $\delta = 2\beta Q/\varepsilon^2$, this identity is confirmed in Fig. 9e.

We recall however, that only the model proposed here accounts for slow dynamics, i.e. it predicts quantitatively the temporal evolution of the offset. The major consequence is that, while the model discussed here allows describing relaxation as well, the hysteretic model fails to do it.

Acknowledgements J. K. acknowledges support from the Technology Agency of the Czech Republic under Grant No. TM04000065. J. K. and R. Z. acknowledge the financial support provided by the Ministry of Education, Youth, and Sports of the Czech Republic via the project No. CZ.02.01.01/00/23_020/0008501 (METEX), co-funded by the European Union and the institutional support of Institute of Thermomechanics through RVO: 61388998.

Author Contributions All authors should confirm their authorship. This can be made, as done in some journals, by sending a mail to each authors asking for confirmation of authorship and agreement for submitting the paper

Funding Open access publishing supported by the institutions participating in the CzechELib Transformative Agreement. No funding was received for conducting this study.

Data Availability The experimental data analysed in the current study are available in the Zenodo repository (Zeman 2025).

Declarations

Conflict of interest The authors have no relevant financial or non-financial interests to disclose.

References

1 Astorga AL, Guéguen P, Rivière J et al (2019) Recovery of the resonance frequency of buildings following strong seismic deformation as a proxy for structural health. Struct Health Monit 18(5–6):1966–1981. https://doi.org/10.1177/1475921718820770

2 Berjamin H, Lombard B, Chiavassa G et al (2018) Modeling longitudinal wave propagation in nonlinear viscoelastic solids with softening. Int J Solids Struct 141–142:35–44. https://doi.org/10.1016/j.ijsolstr.2018.02.009

3 Bittner J, Popovics J (2021) Mechanistic diffusion model for slow dynamic behavior in materials. J Mech Phys Solids 150:104355. https://doi.org/10.1016/j.jmps.2021.104355

4 Favrie N, Lombard B, Payan C (2015) Fast and slow dynamics in a nonlinear elastic bar excited by longitudinal vibrations. Wave Motion 56:221–238. https://doi.org/10.1016/j.wavemoti.2015.02.014

5 Johnson PA, Jia X (2005) Nonlinear dynamics, granular media and dynamic earthquake triggering. Nature 437(7060):871–874. https://doi.org/10.1038/nature04015

6 Kober J, Kruisova A, Scalerandi M (2021) Elastic slow dynamics in polycrystalline metal alloys. Appl Sci 11(18):8631. https://doi.org/10.3390/app11188631

7 Kober J, Scalerandi M, Gabriel D (2023) Robust determination of relaxation times spectra of long-time multirelaxation processes. Phys Rev E 107(3):035302. https://doi.org/10.1103/PhysRevE.107.035302

8 Kober J, Scalerandi M, Zeman R (2023) Non-equilibrium strain induces hysteresis and anisotropy in the quasi-static and dynamic elastic behavior of sandstones: theory and experiments. Appl Phys Lett 122(15):152201. https://doi.org/10.1063/5.0138424

9 Lebedev AV (2023) Slow time phenomena in heterogeneous materials: from microscopic fluctuations to macroscopic relaxation. Acoust Phys 69(1):58–73. https://doi.org/10.1134/S1063771022700543

10 Lebedev AV, Manakov SA (2024) Experimental study of slow sound speed relaxation in carbonate rocks. Acoust Phys 70(2):368–386. https://doi.org/10.1134/S1063771024601638

11 Lebedev AV, Ostrovsky LA (2014) A unified model of hysteresis and long-time relaxation in heterogeneous materials. Acoust Phys 60(5):555–561. https://doi.org/10.1134/S1063771014050066

12 Lee S, Weaver RL (2024) Slow dynamic elasticity at short times. Phys Rev E 109(6):065002. https://doi.org/10.1103/PhysRevE.109.065002

13 McCall KR, Guyer RA (1994) Equation of state and wave propagation in hysteretic nonlinear elastic materials. J Geophys Res Solid Earth 99(B12):23887–23897. https://doi.org/10.1029/94JB01941

14 Ostrovsky L, Lebedev A, Riviere J et al (2019) Long-time relaxation induced by dynamic forcing in geomaterials. J Geophys Res Solid Earth 124(5):5003–5013. https://doi.org/10.1029/2018JB017076

15 Prez-Rfols F, Van Dokkum JS, Nicola L (2023) On the interplay between roughness and viscoelasticity in adhesive hysteresis. J Mech Phys Solids 170:105079. https://doi.org/10.1016/j.jmps.2022.105079

16 Reichhardt CJO, Lopatina LM, Jia X et al (2015) Softening of stressed granular packings with resonant sound waves. Phys Rev E 92(2):022203. https://doi.org/10.1103/PhysRevE.92.022203

17 Remillieux MC, Guyer RA, Payan C et al (2016) Decoupling nonclassical nonlinear behavior of elastic wave types. Phys Rev Lett 116(11):115501. https://doi.org/10.1103/PhysRevLett.116.115501

18 Remillieux MC, Ulrich TJ, Goodman HE et al (2017) Propagation of a finite-amplitude elastic pulse in a bar of Berea sandstone: a detailed look at the mechanisms of classical nonlinearity, hysteresis, and nonequilibrium dynamics: nonlinear propagation of elastic pulse. J Geophys Res Solid Earth 122(11):8892–8909. https://doi.org/10.1002/2017JB014258

19 Rivire J, Renaud G, Guyer RA et al (2013) Pump and probe waves in dynamic acousto-elasticity: comprehensive description

and comparison with nonlinear elastic theories. J Appl Phys 114(5):054905. https://doi.org/10.1063/1.4816395
20 Scalerandi M, Bentahar M, Mechri C (2018) Conditioning and elastic nonlinearity in concrete: separation of damping and phase contributions. Constr Build Mater 161:208–220. https://doi.org/10.1016/j.conbuildmat.2017.11.035
21 Scalerandi M, Mechri C, Bentahar M et al (2019) Experimental evidence of correlations between conditioning and relaxation in hysteretic elastic media. Phys Rev Appl 12(4):044002. https://doi.org/10.1103/PhysRevApplied.12.044002
22 Scalerandi M, Mechri C, Bentahar M et al (2020) Role of slow dynamics in fast dynamics ultrasonic measurements. Commun Nonlinear Sci Numer Simul 91:105452. https://doi.org/10.1016/j.cnsns.2020.105452
23 Sens-Schnfelder C, Snieder R, Li X (2018) A model for nonlinear elasticity in rocks based on friction of internal interfaces and contact aging. Geophys J Int. https://doi.org/10.1093/gji/ggy414
24 Shokouhi P, Rivire J, Guyer RA et al (2017) Slow dynamics of consolidated granular systems: multi-scale relaxation. Appl Phys Lett 111(25):251604. https://doi.org/10.1063/1.5010043
25 Snieder R, Sens-Schnfelder C, Wu R (2017) The time dependence of rock healing as a universal relaxation process, a tutorial. Geophys J Int 208(1):1–9. https://doi.org/10.1093/gji/ggw377
26 TenCate JA (2011) Slow dynamics of earth materials: an experimental overview. Pure Appl Geophys 168(12):2211–2219. https://doi.org/10.1007/s00024-011-0268-4
27 TenCate JA, Shankland TJ (1996) Slow dynamics in the nonlinear elastic response of Berea sandstone. Geophys Res Lett 23(21):3019–3022. https://doi.org/10.1029/96GL02884
28 TenCate JA, Smith E, Guyer RA (2000) Universal slow dynamics in granular solids. Phys Rev Lett 85(5):1020–1023. https://doi.org/10.1103/PhysRevLett.85.1020
29 Vakhnenko OO, Vakhnenko VO, Shankland TJ et al (2004) Strain-induced kinetics of intergrain defects as the mechanism of slow dynamics in the nonlinear resonant response of humid sandstone bars. Phys Rev E 70(1):015602. https://doi.org/10.1103/PhysRevE.70.015602
30 Vakhnenko OO, Vakhnenko VO, Shankland TJ (2005) Soft-ratchet modeling of end-point memory in the nonlinear resonant response of sedimentary rocks. Phys Rev B 71(17):174103. https://doi.org/10.1103/PhysRevB.71.174103
31 Van Den Abeele KEA, Carmeliet J, Ten Cate JA et al (2000) Nonlinear Elastic Wave Spectroscopy (NEWS) techniques to discern material damage, part II: single-mode nonlinear resonance acoustic spectroscopy. Rese Nondestr Eval 12(1):31–42. https://doi.org/10.1080/09349840009409647
32 Van Den Abeele KEA, Johnson PA, Sutin A (2000) Nonlinear Elastic Wave Spectroscopy (NEWS) techniques to discern material damage, part I: nonlinear wave modulation spectroscopy (NWMS). Res Nondestr Eval 12(1):17–30. https://doi.org/10.1080/09349840009409646
33 Van Den Abeele KEA, Sutin A, Carmeliet J et al (2001) Micro-damage diagnostics using nonlinear elastic wave spectroscopy (NEWS). NDT & E Int 34(4):239–248. https://doi.org/10.1016/S0963-8695(00)00064-5
34 Yoritomo JY, Weaver RL (2020) Slow dynamics in a single glass bead. Phys Rev E 101(1):012902. https://doi.org/10.1103/PhysRevE.101.012902
35 Zeman R, Kober J, Nistri F et al (2024) Relaxation of viscoelastic properties of sandstones: hysteresis and anisotropy. Rock Mech Rock Eng. https://doi.org/10.1007/s00603-024-03914-6
36 Kober, J., Scalerandi, M., Tortello, M., Ulrich, T. J., & Zeman, R. (2025). The Role of Fast and Slow Dynamics in Nonlinear Resonant Ultrasound Spectroscopy of Consolidated Granular Materials. Scientific Reports.
37 Zeman, R., Kober, J., & Scalerandi, M. Data for "Distribution of time scales induces slow dynamics and elastic hysteresis in sandstones: A model of non-equilibrium strain", *Zenodo*, v1, https://doi.org/10.5281/zenodo.15524423 (2025).
38 Li X, Sens-Schönfelder C, Snieder R (2018) Nonlinear elasticity in resonance experiments Physical Review B Condensed Matter and Materials Physics, 144301, 1-9. https://doi.org/10.1103/PhysRevB.97.144301